Suppression of Electron Thermal Conduction by Whistler Turbulence in a Sustained Thermal Gradient

G. T. Roberg-Clark, J. F. Drake, C. S. Reynolds, and M. Swisdak

Suppression of electron thermal conduction by whistler turbulence in a sustained thermal gradient

G. T. Roberg-Clark,[1, *] J. F. Drake,[1, 2, 3, 4, †] C. S. Reynolds,[5, 4, ‡] and M. Swisdak[1, 3, 4, §]

[1]*Department of Physics, University of Maryland College Park, College Park, MD 20740, USA*
[2]*Institute for Physical Science and Technology, University of Maryland, College Park, MD 20742, USA*
[3]*Institute for Research in Electronics and Applied Physics,*
University of Maryland, College Park, MD 20742, USA
[4]*Joint Space-Science Institute (JSI), College Park, MD 20742, USA*
[5]*Department of Astronomy, University of Maryland College Park, College Park, MD 20740, USA*
(Dated: November 13, 2017)

The dynamics of weakly magnetized collisionless plasmas in the presence of an imposed temperature gradient along an ambient magnetic field is explored with particle-in-cell simulations and modeling. Two thermal reservoirs at different temperatures drive an electron heat flux that destabilizes off-angle whistler-type modes. The whistlers grow to large amplitude, $\delta B/B_0 \simeq 1$, and resonantly scatter the electrons, significantly reducing the heat flux. A surprise is that the resulting steady state heat flux is largely independent of the thermal gradient. The rate of thermal conduction is instead controlled by the finite propagation speed of the whistlers, which act as mobile scattering centers that convect the thermal energy of the hot reservoir. The results are relevant to thermal transport in high β astrophysical plasmas such as hot accretion flows and the intracluster medium of galaxy clusters.

Introduction. Thermal conduction is integral to a wide variety of phenomena occurring in space and astrophysical plasmas. Ascertaining the rate of thermal conduction in such systems is therefore of fundamental importance. In particular, the microphysics of weakly collisional, weakly magnetized plasmas, which is not fully understood, may play a pivotal role in determining the transport properties of the global system [1]. A magnetic field makes thermal conduction anisotropic and when the plasma β is greater than order unity, the system is susceptible to a host of microscale kinetic instabilities which tend to suppress thermal fluxes via particle scattering [2–7]. Such instabilities are expected to operate in rarefied plasma environments such as the Intracluster Medium (ICM) of galaxy clusters [8–10] as well as hot accretion flows [11, 12] and the solar wind [13–15].

The impact of instabilities on transport is tied to their nonlinear evolution, which in turn is influenced by the input of free energy from the surrounding astrophysical environment that can be included through appropriate boundary conditions in numerical models. Examples include those used in shearing-box [7, 16] and compressing-box [17, 18] simulations of instabilities driven by pressure anisotropies and their impact on the transport of heat and momentum in accretion flows. Here we focus on the dynamics of a system in contact with two thermal reservoirs at different temperatures, driving a heat flux parallel to an ambient magnetic field. We use particle-in-cell (PIC) simulations to model the resulting heat flux instability and steady-state suppressed thermal conduc-

tion with a sustained thermal gradient. This model is in contrast to previous work in which the heat flux instability was studied as an initial value problem [10].

Numerical Scheme. We carry out two-dimensional (2D) simulations using the PIC code `p3d` [19] to model thermal conduction along an imposed temperature gradient in a magnetized, collisionless plasma with open boundaries. `p3d` calculates particle trajectories using the relativistic Newton-Lorentz equations and the electromagnetic fields are advanced using Maxwell's equations. The ends of the simulation domain act as thermal reservoirs at two different temperatures $T_h > T_c$ separated by a distance L_x, forming a temperature gradient $T' \equiv (T_h - T_c)/L_x$ and driving a heat flux. An initially uniform magnetic field $\mathbf{B_0} = B_0\hat{\mathbf{x}}$ threads the plasma along the gradient and is free to evolve in time. The initial particle distribution function is chosen to model the free-streaming of particles from each thermal reservoir and has the form

$$f(\mathbf{v}, t = 0) = f_h + f_c$$
$$= \frac{n_0}{\pi^{3/2}} \left(\frac{e^{-v^2/v_{Th}^2}}{v_{Th}^3}\theta(v_\parallel) + \frac{e^{-[(v_\parallel+v_d)^2+v_\perp^2]/v_{Tc}^2}}{v_{Tc}^3(1 + \mathrm{erf}(v_d/v_{Tc}))}\theta(-v_\parallel) \right) \quad (1)$$

where n_0 is the initial density, θ is the Heaviside step function, $v_T = \sqrt{2T/m}$ is the thermal speed, and the parallel and perpendicular directions are with respect to $\mathbf{B_0}$. The cold particles are given a parallel drift speed v_d to ensure zero net current ($\langle v_\parallel \rangle = 0$) in the initial state while the error function $\mathrm{erf}(v_d/v_{Tc})$ makes the density of hot and cold particles equal. f_0 also has nonzero pressure anisotropy ($\langle v_\parallel^2 \rangle \neq \langle v_\perp^2/2 \rangle$) and a heat flux $q_\parallel = \langle v_\parallel v^2 \rangle = q_0$. f_0 is not unstable in a 1D system since only off-angle modes resonate with particles near the large phase space discontinuity in f_0 at $v_\parallel = 0$ (Fig. S1a).

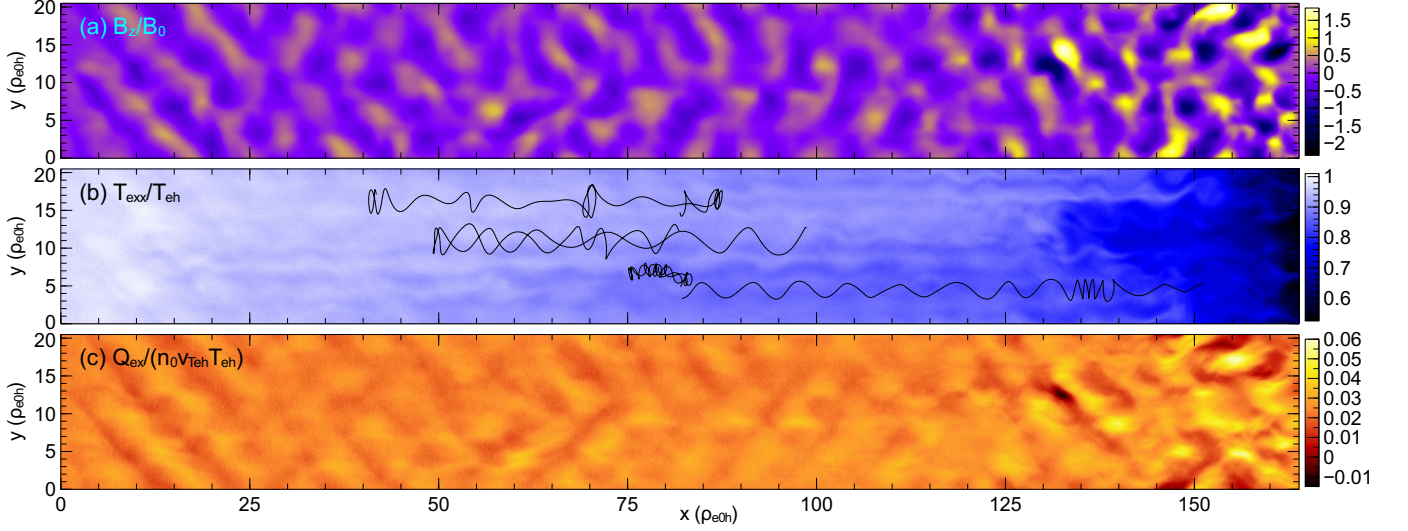When particles exit the open boundaries they are re-

FIG. 1. Two dimensional plots from the largest simulation ($L_x = 2L_0$) in a saturated state at $t = 800 \, \Omega_{e0}^{-1}$. (a) Fluctuations in out-of-plane B_z (b) Temperature T_{exx} with four self-consistent particle trajectories overlaid. (c) Heat flux q_{ex}.

injected with velocities pulled from f_h (at $x = 0$) or f_c ($x = L_x$). The drift velocity v_d is then recalculated at each time step to ensure that the current of re-injected particles cancels the current of outgoing particles at the cold reservoir. The electromagnetic field components at the thermal reservoir boundaries are $F_y = 0$, $\partial F_x/\partial x = \partial F_z/\partial x = 0$ where $F = (\mathbf{E}, \mathbf{B})$. Periodic boundary conditions are used for both particles and fields in the y direction. Ions in the simulation are not evolved in time and act as a charge-neutralizing background. The subscript e denotes an electron quantity.

Table 1			
L_x	β_{e0h}	T_{ec}/T_{eh}	$q_{ex,f}/(n_0 v_p T_{eh})$
$L_0 = 82 \, \rho_{e0h}$	64	1/2	3.44
$L_0/2$	64	1/2	3.30
$2L_0$	64	1/2	3.26
L_0	32	1/2	3.46
L_0	128	1/2	3.19
L_0	64	1/4	2.56

Simulation Parameters. We have performed six simulations in which L_x, B_0 and T_{ec}/T_{eh} are varied independently so as to change T' and $\beta_{e0h} = 4\pi n_0 T_{eh}/(B_0^2/2)$. The baseline simulation has $L_x = L_0 = 82 \, \rho_{e0h}$, $\beta_{e0h} = 64$, $T_{ec} = T_{eh}/2$, $\omega_{pe}/\Omega_e = 40$, and $T_{eh}/(m_e c^2) = .02$, where $\rho_{e0h} = v_{Teh}/\Omega_{e0}$ is the gyroradius, $\Omega_{e0} = eB_0/(m_e c)$ is the cyclotron frequency, and $\omega_{pe} = (4\pi n_0 e^2/m_e)^{1/2}$ is the plasma frequency. The parameters for each simulation are listed in Table 1. Each simulation uses 560 particles per cell, has a transverse length L_y of 20 ρ_{e0h}, and is run to $t = 800 \, \Omega_{e0}^{-1}$. The largest simulation ($L_x = 2L_0$) has a spatial domain of 32768 by 4096 grid cells.

Whistler Turbulence. Initializing the simulations with f_0 leads to an impulse of transient fluctuations in the

out-of-plane magnetic field B_z that propagate towards the hot thermal reservoir (evidence for this is shown later). These fluctuations are driven by the initial pressure anisotropy and quickly lead to a sharp drop in the anisotropy to the marginally stable level for firehose-type modes (not shown). The fluctuations rapidly damp and become dynamically unimportant in the simulations and are not discussed further.

The reinjection and mixing of hot and cold particles results in a continuous source of heat flux in the simulation domain. The heat flux drives off-angle ($k_y \simeq k_x$), slowly propagating ($\omega/k \ll v_{Teh}$), elliptically polarized whistler modes that reach large amplitude, $\delta B/B_0 \simeq 1$ (fig. 1a), and strongly scatter electrons, isotropizing the electron distribution function (see the supplementary material). The heat flux q_{ex} drops well below its initial value q_{ex0}. Some reflection of waves occurs at the cold plate boundary but the heat flux is insensitive to the length of the simulation domain, confirming that such reflection does not impact the integrated results.

Strong scattering by the whistlers causes inherently 2D structures to develop in quantities such as the temperature $T_{exx} = m_e \langle v_x^2 \rangle$ (figure 1b) and heat flux q_{ex} (figure 1c). In figure 1b the trajectories of four electron macroparticles from the simulation, tracked starting from an initial position $x = L_x/2$ for a period of 87.5 Ω_{e0}^{-1} in steady state, are overlaid over T_{exx}, which does not vary appreciably during the time of the orbits. Some particles reverse their parallel velocity several times as a result of scattering in the strong magnetic fluctuations. Because the system is 2D the particle out-of-plane canonical momentum, $p_{ez} = m_e v_z - eA_z$, is a conserved quantity. Since $A_z \sim yB_x$ and kinetic energy is mostly conserved in the magnetic fluctuations, the electrons are confined to relatively narrow channels in y.

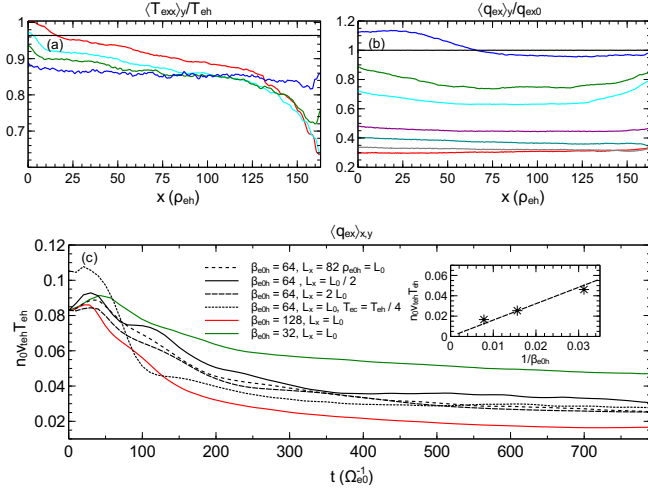*Suppression of Thermal Conduction.* Suppression of

FIG. 2. Temperature and heat flux profiles. (a) Line plots of y-averaged T_{exx} for the run with $L_x = 2L_0$ at times $t\Omega_{e0} = 0$ (black), 80 (blue), 200 (green), 400 (cyan), and 800 (red). (b) Line plots of y-averaged heat flux at times $t\Omega_{e0}^{-1} = 0$ (black), 30 (blue), 100 (green), 150 (cyan), 300 (purple), 450 (grey-blue), 600 (grey), and 800 (red). (c) Box-averaged $\langle q_{ex}(t)\rangle_{x,y}$ for the six simulations in Table 1. *Inset*: Linear fit to the steady state heat flux $q_{ex,f}$ as a function of $1/\beta_{e0h}$.

the heat flux develops over a time of hundreds of Ω_{e0}^{-1} resulting in a steady state in which a continuous temperature profile has formed between the hot and cold reservoirs (fig. 2a) and the heat flux has leveled off to a nearly constant value (fig. 2b). Fig. 2c shows the time profiles of average heat flux $\langle q_{ex}\rangle_{x,y}$ for six simulations. The expectation for a system subject to Coulomb scattering (or another scattering process) is that the heat flux is diffusive, $\mathbf{q}_e \propto -\nabla T_e$. We find instead that the final heat flux is insensitive to the ambient gradient. The black lines in fig. 2c correspond to simulations with a fixed $\beta_{e0h} = 64$ but differing box lengths or hot to cold temperature jumps. For all of these runs the heat flux settles at around $0.03\, n_0 T_{eh} v_{Teh}$. Thus, the heat flux rather than the gradient controls the dynamics. As long as T_{eh} is significantly greater than T_{ec}, the hot plate controls the final heat flux. However, the two simulations with differing β_{e0h} have noticeably different asymptotic heat fluxes that follow the scaling $\langle q_{ex}\rangle_{x,y} \propto 1/\beta_{e0h}$ (fig 2c inset). To explain this result we turn to the physics of scattering by large-amplitude whistler waves.

Scattering by Whistlers. The physics of resonant interactions of particles with elliptically polarized whistlers is well-documented in the literature (see e.g. [10] and references therein). In the frame of a single off-angle whistler wave, total kinetic energy is conserved and particles which satisfy the various resonance criteria $v_{\parallel} = n\Omega_0/k, n = 0, \pm1, \pm2, ...,$ are trapped [20]. For $\delta B/B_0 \ll 1$, resonant particles experience small oscillations in the $v_{\parallel}/v_{\perp}$ plane. For large-amplitude whistlers ($\delta B/B_0 \gtrsim 0.3$) resonances can overlap, leading to irreversible diffusive behavior along circular, constant energy
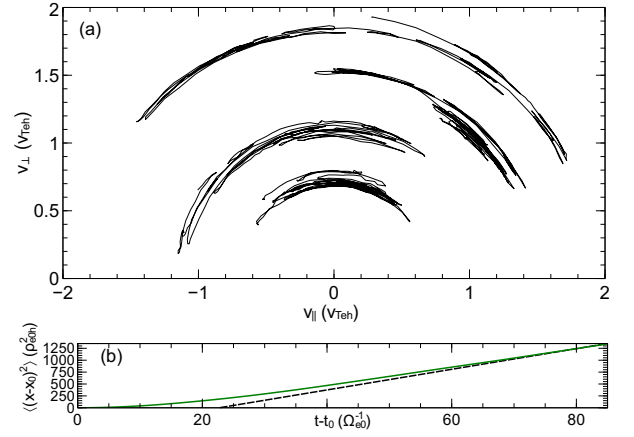

FIG. 3. Evidence for scattering of electrons by whistlers. (a) Trajectories of particles in $v_{\parallel}, v_{\perp}$ space showing significant deflection of pitch angle $\phi = \tan^{-1}(v_{\perp}/v_{\parallel})$. (b) Plot of $\langle(x(t) - x(t_0))^2\rangle$ with linear fit to the slope representing diffusion coefficient D.
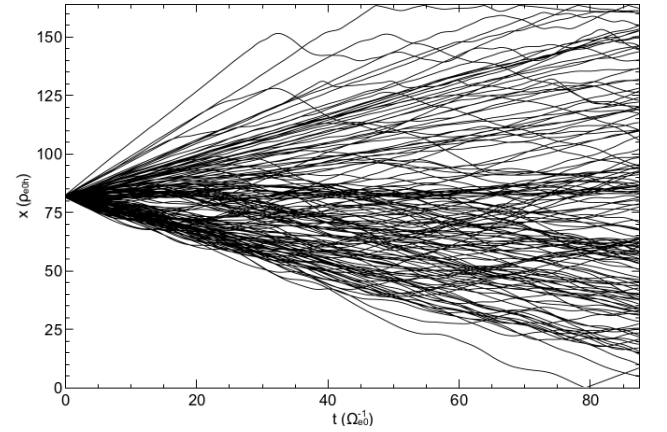

FIG. 4. Line plots of $x(t)$ for 150 particles in the $L_x = 2L_0$ simulation indicating diffusive behavior.

curves in the whistler wave frame [20]. In the presence of multiple whistlers with differing parallel phase speeds some diffusion may also occur perpendicular to circles of constant energy [20]. Resonance overlap is an effective mechanism for heat flux suppression since it causes large deflections in the particle pitch angle $\phi = \tan^{-1}(v_{\perp}/v_{\parallel})$, quenching the parallel heat flux [10].

To demonstrate that this is the physics at play in our simulations, in fig. 3a we show a resonance diagram in $v_{\parallel} - v_{\perp}$ for four trapped particles with differing energy in the simulation with $L = 2L_0$ at steady state. Particle energy is mostly conserved and the primary diffusion is in pitch angle [20]. All the particles display significant deflection so the bulk of particles undergo trapping by the whistlers. Also of note is that the nearly-circular contours in velocity space are effectively centered about $v_{\parallel} = 0$, indicating that the whistler phase speed is small compared to the thermal speed v_{Teh}.

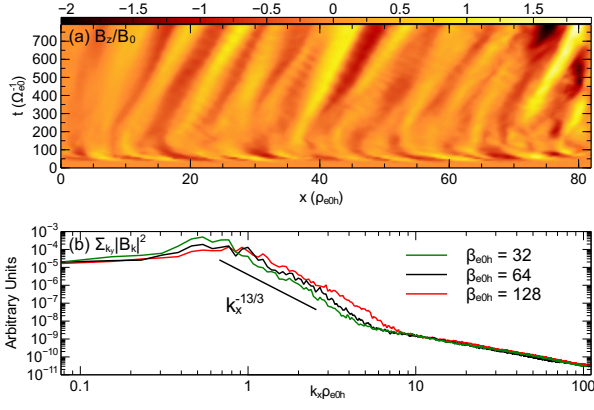To quantify the rate of scattering by the whistlers

FIG. 5. (a) Spacetime plot (t versus x) of whistler fluctuations propagating through the simulation with $L_x = L_0, \beta_{e0h} = 64$ at $L_y/2$. At early times the initial condition f_0 produces fluctuations that reverse direction and are overtaken by the whistlers, which then move to the right. The fluctuations move slowly compared to the thermal speed and most do not reach the cold reservoir at $x = L_0$ by the end of the simulation at $t = 800\,\Omega_{e0}^{-1}$. (b) Fourier spectra, summed over k_y and plotted as a function of k_x for the simulations with $L_x = L_0$ and $\beta_{e0h} = 32, 64,$ and 128.

we calculate the quantity $\langle (x(t) - x(t_0))^2 \rangle$ by averaging over individual trajectories of roughly 8000 particles for the $L_x = 2L_0$ simulation (fig. 3b). The diffusion rate $D = \langle v^2 \rangle \tau$ is half the linear slope of $(x - x_0)^2$ at late time, where τ is the scattering time. We find $\tau \simeq 6.80\Omega_{e0}^{-1}$. We plot x versus time for 150 particles in fig. 4 to illustrate the particle motion. Some particles are diverted back towards the initial particle location at $y = L_0$ once scattering becomes significant while others maintain their initial direction of propagation. The linear trend of mean-squared displacement in 3b is evidence for diffusive behavior. Pitch angle scattering in a spectrum of whistler turbulence was also reported by [21].

Steady State Heat Flux. The results of fig. 2a have demonstrated that the asymptotic rate of thermal conduction in the presence of large-amplitude whistler waves is largely independent of the temperature gradient and instead follows a scaling $1/\beta_{e0h}$. A simple explanation for this result, consistent with a comment in [3], is that whistlers act as particle scattering centers that propagate at their phase speed $v_p = \omega/k$ and control the net flow of high-energy particles carrying the bulk of the heat flux. The resulting heat flux is simply the product of the phase speed and the thermal energy of the hot plasma, $q_{ex} \sim n_0 v_p T_{eh}$.

The whistler wave phase speed is determined via the cold plasma dispersion relation, $\omega = k^2 \rho_e^2 \Omega_e / \beta_e$. Taking $k\rho_e \sim 1$ (as in [10]) for whistlers at high β_e, we find

$$\frac{\omega}{k} \sim \frac{v_{Te}}{\beta_e}. \tag{2}$$

In figure 5a we show a spacetime diagram (t versus x) of the out-of-plane B_z at a single value of $L_y/2$. After

a transient associated with the anisotropy-driven waves of the initial distribution f_0 that was discussed earlier, the whistlers propagate at a nearly uniform speed in the direction of $-T'$ ($+\hat{x}$). To confirm that the unstable modes have $k\rho_e \sim 1$, we show the power spectrum $|B_{k_x}|^2$ for the runs with $L_x = L_0$ at $\beta_{e0h} = 32, 64$ and 128 in fig. 5b. The spectra are nearly isotropic in the 2D Fourier space $k_x - k_y$ (not shown) so in the spectra shown the energy has been summed over k_y. We find a spectral index of $-13/3$ for the modes near $k_x \rho_{e0h} = 1$ although we note that the more important point is to establish that the spectrum peaks near $k\rho_{e0h} = 1$ even as β_{e0h} varies. A more complete exploration of the spectrum requires simulations with a third spatial dimension. In addition we find that for each of the six simulations in Table 1, $q_{ex,f} \simeq 3\,n_0 v_p T_{eh}$, where v_p was measured in the middle of the simulation domain. These results strongly support the scaling

$$q_{\parallel} = \alpha n_0 \frac{\omega}{k} T_{eh} \sim n_0 \frac{v_{Teh}^3}{\beta_{e0h}} = v_{Teh} \frac{B_0^2}{2}, \tag{3}$$

where α is a coefficient of order unity. Equation (3) reveals the crucial role of the background magnetic field in facilitating thermal transport since it controls the propagation of whistlers. In the case of a very small magnetic field the whistlers barely propagate and the thermal conduction is virtually shut off. However, no whistler growth was found in a simulation with $B_0 = 0$ (not shown), indicating that heat flux suppression by whistlers requires a finite ambient magnetic field. Recent PIC simulations with an imposed thermal gradient suggest that pressure anisotropy driven modes are at play when there is no initial ambient magnetic field [22]. Those results are consistent with the transient growth of fluctuations seen in our simulations in the case of $B_0 = 0$. These reach finite amplitude but then rapidly decay on time scales short compared with the development of the heat-flux instability.

Discussion. A caveat of our model is that the imposed thermal gradient is much larger than that measured in environments such as the ICM [3]. However, the present simulations suggest that the transport is insensitive to the imposed temperature gradient (although the sign of the parallel heat flux is determined by the sign of $-\nabla T_e$ through the whistler phase speed). The point is that heat flux instability is directly driven by the collisionless heat flux, which depends only on the temperature difference across a domain, rather than the ambient gradient. It seems likely, therefore, that the current results apply to cases in which the temperature gradient is far weaker. A full treatment of the ICM also requires the inclusion of weak collisions not present in our kinetic model.

A question is how the microphysics of whistler scattering will affect heating and thermal conduction in the intracluster medium. The scaling of heat flux in (3) with $1/\beta_e$ implies a suppression factor of roughly 100 below the free-streaming thermal conduction. The functional dependence $q_{\parallel} \propto T^{1/2}$ is a noticeable departure from

the Spitzer conductivity [23] proportional to $T^{7/2}$ often used in hydrodynamic or MHD models of the ICM (e.g. [24], [25]). Our results may therefore significantly alter the equilibria associated with clusters of galaxies, which result from a balance between thermal conduction and radiative cooling.

Our results show promising similarities with the observations of thermal conduction in the solar wind by Bale et al. [26] in which the heat flux takes on a constant value, independent of collisionality and the ambient temperature gradient, in the weak collisionality regime where the collisional mean-free-path exceeds the temperature scale length. However, much of their data is in a regime of much lower β than in the present simulations. The exploration of the transition from high to low β with analysis and simulations is underway so that more detailed comparisons with solar wind observations can be made.

[1] F. Rincon, A. A. Schekochihin, and S. C. Cowley, MNRAS **447**, L45 (2014).

[2] A. Ramani and G. Laval, Physics of Fluids **21**, 980 (1978).

[3] A. Levinson and D. Eichler, The Astrophysical Journal **387**, 212 (1992).

[4] S. P. Gary and H. Li, The Astrophysical Journal **529**, 1131 (2000).

[5] M. W. Kunz, A. A. Schekochihin, and J. M. Stone, Physical Review Letters **112**, 1 (2014).

[6] S. V. Komarov, E. M. Churazov, M. W. Kunz, and A. A. Schekochihin, MNRAS **477**, 467 (2016).

[7] M. A. Riquelme, E. Quataert, and D. Verscharen, The Astrophysical Journal **824** (2016).

[8] A. A. Schekochihin, S. C. Cowley, F. Rincon, and M. S. Rosin, MNRAS **405**, 291 (2010).

[9] M. W. Kunz, A. A. Schekochihin, S. C. Cowley, J. J. Binney, and J. S. Sanders, MNRAS **410**, 2446 (2011).

[10] G. T. Roberg-Clark, J. F. Drake, C. S. Reynolds, and M. Swisdak, The Astrophysical Journal **830**, L9 (2016).

[11] E. Quataert, The Astrophysical Journal, Volume 500, Issue 2, pp. 978-991. **500**, 978 (1997).

[12] P. Sharma, E. Quataert, G. W. Hammett, and J. M. Stone, The Astrophysical Journal **667**, 714 (2007).

[13] P. Hellinger and P. M. Trávníček, Journal of Geophysical Research: Space Physics **118**, 5421 (2013).

[14] J. V. Hollweg, Journal of Geophysical Research **79**, 3845 (1974).

[15] S. P. Gary, E. E. Scime, J. L. Phillips, and W. C. Feldman, Journal of Geophysical Research **99**, 23391 (1994).

[16] M. W. Kunz, J. M. Stone, and E. Quataert, Physical Review Letters **117**, 1 (2016).

[17] L. Sironi and R. Narayan, The Astrophysical Journal **800**, 88 (2015).

[18] L. Sironi, The Astrophysical Journal **800** (2015).

[19] A. Zeiler, D. Biskamp, J. F. Drake, B. N. Rogers, M. A. Shay, and M. Scholer, Journal of Geophysical Research **107**, 1230 (2002).

[20] H. Karimabadi, D. Krauss-Varban, and T. Terasawa, Journal of Geophysical Research **97**, 13853 (1992).

[21] B. D. Keenan and M. V. Medvedev, Journal of Plasma Physics **82**, 905820207 (2016).

[22] K. M. Schoeffler, N. F. Loureiro, and L. O. Silva, arXiv preprints (2017), arXiv:1707.06069v1.

[23] L. Spitzer, *Physics of Fully Ionized Gases*, 2nd ed. (New York: Interscience, 1962).

[24] M. Ruszkowski and S. P. Oh, The Astrophysical Journal **713**, 1332 (2010).

[25] H.-Y. K. Yang and C. S. Reynolds, The Astrophysical Journal **818**, 181 (2016).

[26] S. D. Bale, M. Pulupa, C. Salem, C. H. K. Chen, and E. Quataert, The Astrophysical Journal **769**, L22 (2013).